2017 CEM Research for Undergraduates Journal

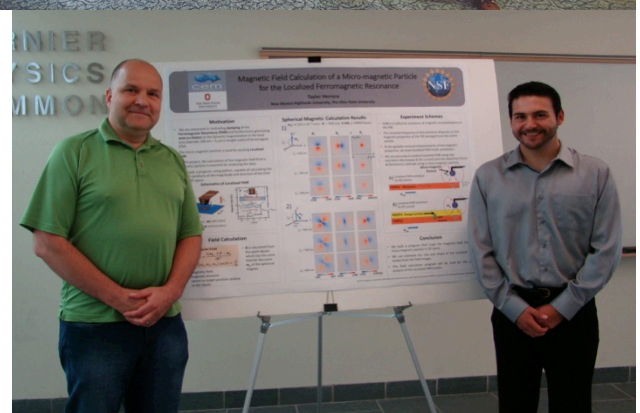

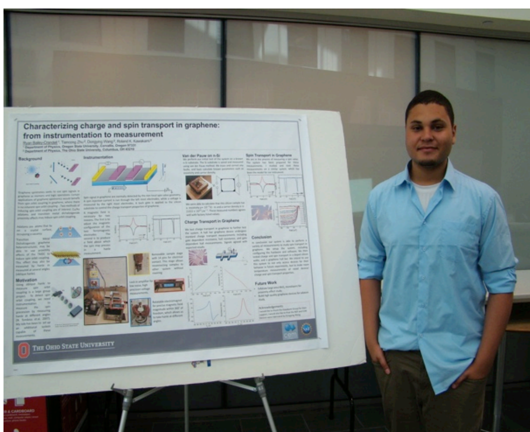

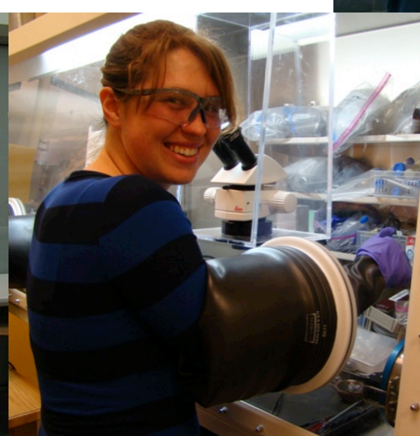

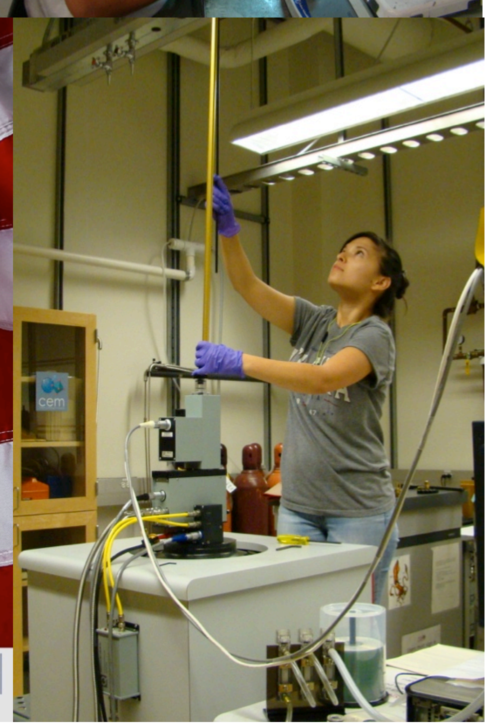

Table of Contents

Characterization of a Micro-magnetic Particle for the Localized Ferromagnetic Resonance

Taylor Herrera
Department of Physics, The Ohio State University, Columbus, OH 43210, USA
(Dated: July 7, 2017)

ABSTRACT

We calculate magnetic fields emanating from a point dipole and create their maps in a 3-dimensional space. When a DC current flows through a bilayer system of ferromagnetic (FM) and normal metal (NM), the spin-orbit interaction on its interface causes the spin torque exerted on the FM. Above the certain threshold current, it can induce an auto-oscillation of a coherent magnetization precession, the same phenomenon observed in ferromagnetic resonance by applying a microwave field. We are interested in observing the auto-oscillation of FMR modes localized by a dipolar field generated from a micron-sized magnetic particle in the bilayer films consisting of the permalloy(Py, FM) and platinum(Pt, NM). In this project, the calculation of the magnetic field from a magnetic particle is essential for analyzing the data. Here we make a program that calculates a point dipole field and constructs its 3D map using a Python, assuming that our magnetic particle in a spherical shape has the same field from a point dipole with the same magnetic moment. The program is capable of imaging the magnitude and direction of the field in our assigned 3D space and the dipole in our calculation can be located at any position that we want.

INTRODUCTION

We are interested in auto-oscillation of a ferromagnet due to spin-orbit torques in response to a dc current that can generate controllable high frequency magnetic dynamics. The program is useful for scanned magnetic probe experiments. Ferromagnetic Resonance(FMR) is a method to measure magnetic properties by detecting the processional motion of the magnetization in a ferromagnetic sample. [1] In Figure 1 this is an example of using a microwave to create FMR using a probe and a sample. The same thing, Figure 2, can be achieved by using a DC current through a normal metal, platinum and a ferromagnet. The current through the normal metal creates a spin polarized current. We can conduct experiments such as Localized Mode FMR and Spin Torque FMR for example.

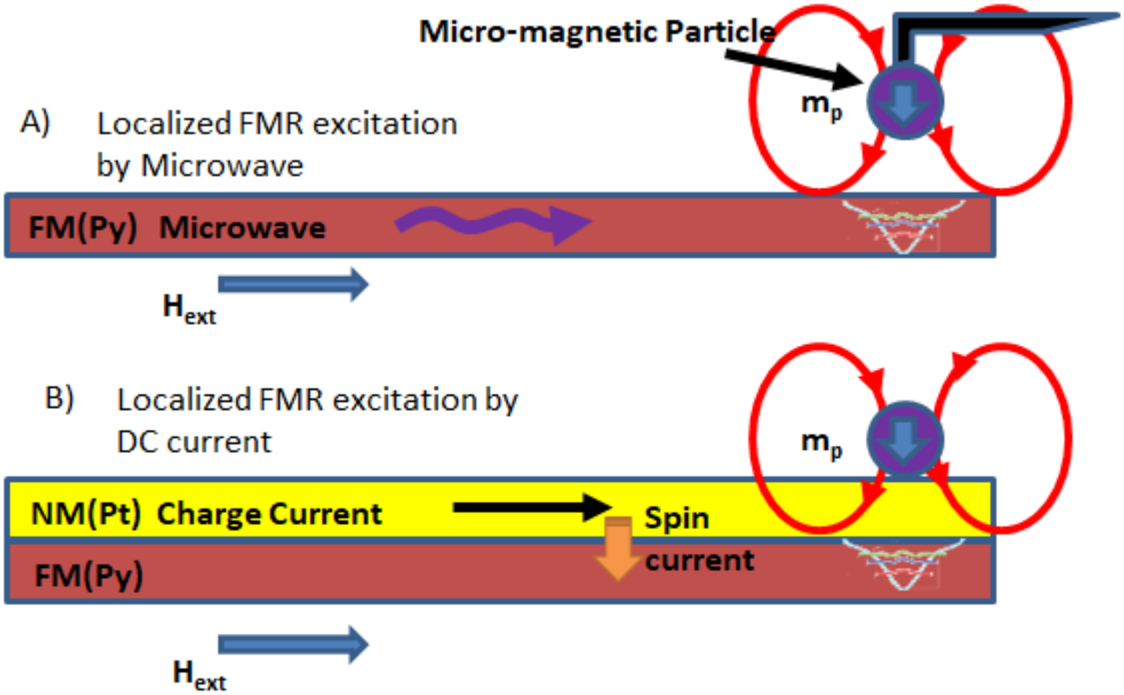

Localized Mode FMR is achieved by combining a probe magnet and a local magnetic field which makes the magnetic resonance excited in the entire sample. When the probe is close to the sample, we create a strong magnetic field. This changes the oscillations that are in the vicinity of the probe. The oscillations are defined by the local property of the probe. Resonance frequency depends on the form of the material. If we have variations of magnetic properties in the sample, we are able to map them because putting the probes in the same magnetic field the resonance frequency of precession will be different depending on the local properties of materials.

Spin Torque FMR is achieved by generating the spin polarized current which exerts an anti-damping torque on the magnetization of the FM. This spin polarized current is generated at the interface of FM/NM due to the strong spin orbit interaction in the NM such as in platinum(Pt).

METHODS

We installed Python version 2.7.12 on Windows to create a program that calculates a point dipole field and construct a 3D map. After installing python, we used pip to install the Matplotlib library to graph our results. In order to see how our results were changing in real time, we used the integrated development environment(IDE) debugger mode. When everything is installed, we started on our first program which calculated a single dipole field point. This program simulates placing a dipole at a specific point in a 2D plane. After we compared our results with a matlab program that has our expected results. We started to work on making a dipole field map. This map is capable of creating a 3D representation of our dipole field. This is useful to see how the magnitude and direction of the fields. We are interested in seeing Bx, By, and Bz which are vectors in the point dipole that represent the magnetic field. The units we used are Gaussian because all equations were measured in that unit.

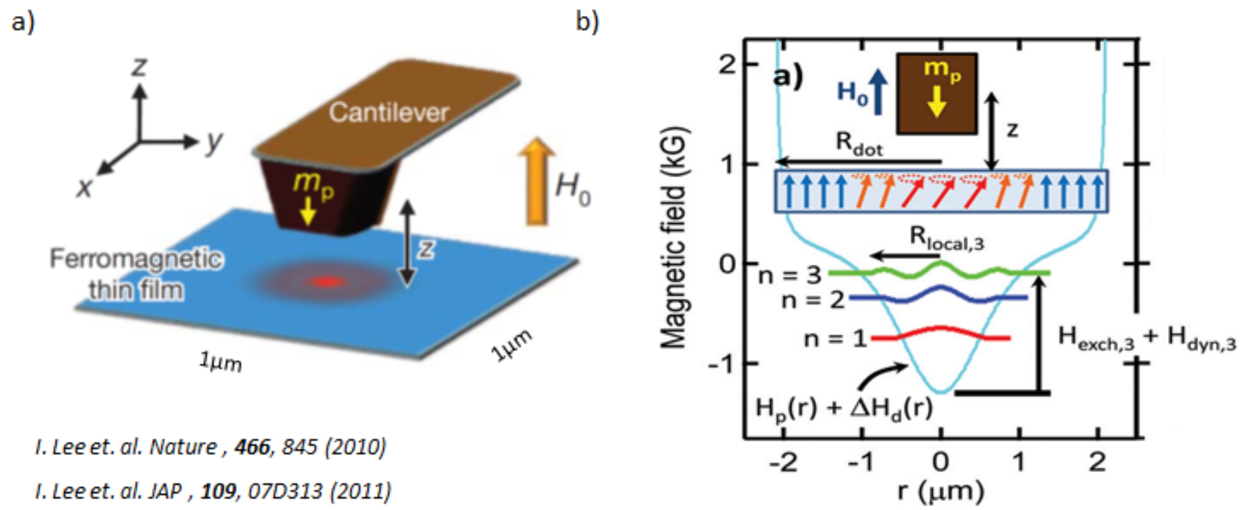

This is the schematics of the localized FMR. We can excite FMR signals locally by supplying addition field, the probe magnet. The resonance condition is only satisfied in the loacalized area. The red area is where the spins are excited.

RESULTS

Figure 1.

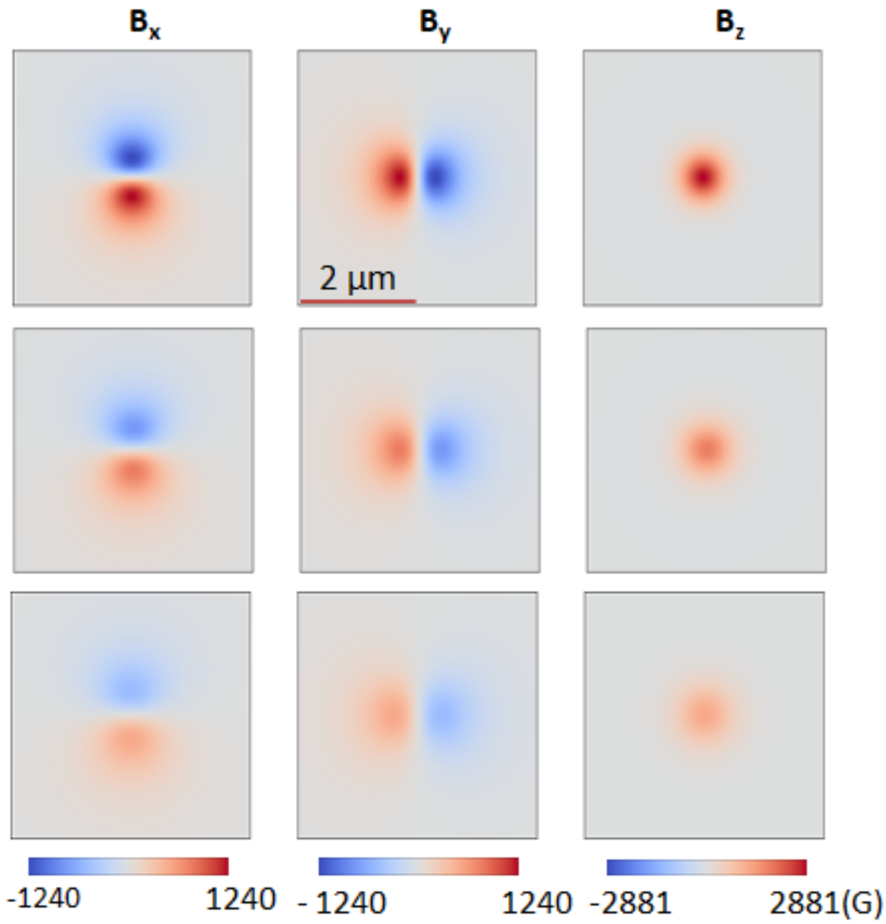

In Figure 1 we put our dipole field calculation in an X and Y plane with the sample size scale being four microns by four microns. As the distance from the magnetic particle to the increases, the magnetic field decreases.

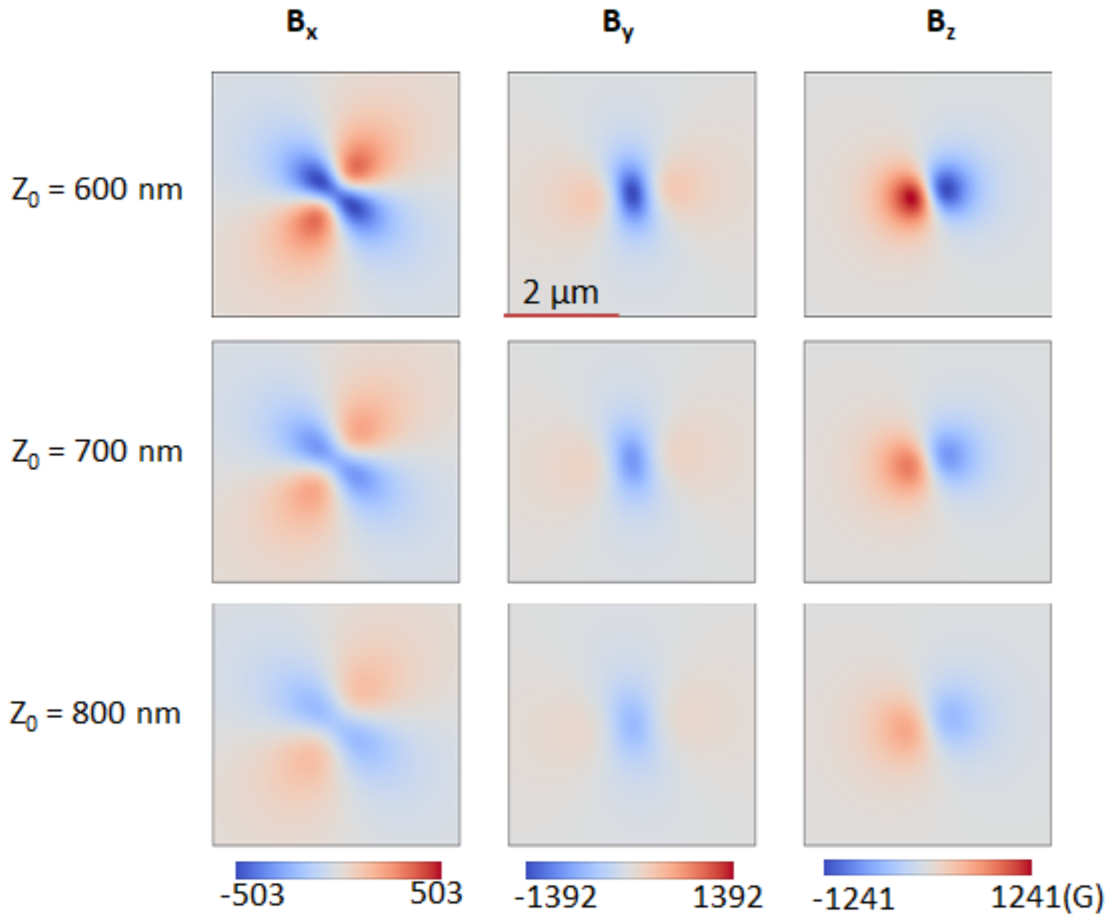

In Figure 2 we replicated the experiment, the difference is we added a 75° angle to the magnetic moment of the micro magnetic particle. We see the same results as in Figure 1 as we expected.

Knowing that our program is correct, we can add any arbitrary to the magnetic moment. This program is essential for our future data analysis because it will estimate the size of our magnetic field.

CONCLUSION

We successfully created a program that simulates the magnetic moment of a spherical micro magnetic particle. The program is capable of giving the intensities of the magnetic field at any arbitrary angle. Our future goals for this experiment is to an electrical current through a normal metal with strong orbit interactions that will be converted to spin current into a ferromagnet and localize the FMR, as opposed to using a localizing the FMR using microwave.

ACKNOWLEDGMENTS

I want to thank Inhee, Denis, and Chris Hammel for the moral support and their advisement. They were supportive with my research and learning experience.

REFERENCES

[1]Wolfgang Kuch, Ferromagnetic Resonance(FMR), Physik.fu-berlin.de (2017).

*I. Lee et. al. JAP , **109**, 07D313 (2011)*
*I. Lee et. al. Nature , **466**, 845 (2010)*

Digital Image Analysis of Micro/Nanostructures within Dentin

James M. Kuznar[1], Isabel N. Boona[1], David W. McComb[1]

[1]Center for Electron Microscopy and Analysis, Material Science and Engineering, The Ohio State University, Columbus, OH

28 July 2017

Abstract

There are three main layers to teeth. Enamel is the outermost layer followed by dentin and pulp. Dentin is produced by odontoblasts [1] which are cells located in the pulp of the tooth. Dentin is a composite material that mainly contains inorganic hydroxyapatite crystals ($Ca_5(PO_4)_3(OH)$) and organic collagen matrix proteins [1]. Dentin contains microtubular structures that are present throughout at varying quantities and diameters [2]. Some of these microtubules have channel like structures that branch out from the tubules through the peritubular dentin and in some cases to other microtubules. These channel-like structures are referred to as 'nanotubules'. This research seeks to better visualize the dentin tubules and peritubular dentin. How these micro and nano tubule features are positioned relative to each other can potentially provide significant insight into the diffusion of ionic species throughout the intertubular dentin in three-dimensional (3D) space.

Introduction

There is interest in dentin because of its role in hypersensitivity which affects anywhere from 10% to 30% of the general population [5]. Dentin hypersensitivity (DH) is characterized as short sharp pain and can be caused by stimuli such as mechanical, chemical, and thermal with the latter being the most common [5]. For DH to occur, the dentin needs to be exposed. Both loss of enamel and a receding gum line exposes dentin [5]. Acidic foods can lead to enamel loss and excessive brushing can recede the gum line. The most widely accepted explanation for dentin hypersensitivity is the hydrodynamic theory which states that as fluid moves within dentin tubules it stimulates nerves in the pulp [4,5]. The two main methods for addressing the symptoms of dentin hypersensitivity include numbing agents that interfere with the transmission of the pain signal and occluding agents which fill in or seal the most exposed part of the dentin [4,5].

Because of the constant stress and release it experiences during chewing, dentin's mechanical properties are an area of active research. Man-made restoration of human teeth, in the form of dental repair or replacement, does not perform as well as natural dentin [7]. There is some evidence that most of the mechanical properties of dentin are due to the orientation of the tubules [7].

The micro/nanostructures need to be thoroughly investigated and visualized to increase the effectiveness of occluding agents as well as understand the contributing factors to dentin's mechanical properties. Thus, this research is focused on creating and manipulating 3D reconstructions of the various microstructures within dentin using various image processing techniques.

Experimental Method

A 50 micron diameter cylinder of dentin was removed from a bulk human tooth using a Plasma focused ion beam Dual Beam™ (PFIB) at Thermo Fisher Scientific in Hillsboro, OR. The dentin cylinder was non-destructively scanned using computed tomography (CT) on a Zeiss Ultra nano-CT instrument at a resolution of 110 nm. CT involves an X-ray source, detectors, and a rotating sample [3]. The different microstructures within dentin have varying densities which "attenuate the incident X-ray beam to varying amounts" [3] allowing them to be differentiated from each other. The CT scan of the human dentin piece was reconstructed using a back-filtered mathematical algorithm and viewed as a 3D reconstruction. The 3D reconstruction was then exported as TIF images into horizontal slices of the dentin each with a depth of 0.0637255 µm.

The data then underwent segmentation, or the "separation of data into disjoint regions" [6]. A 2D/3D processing/analytical package called MIPAR™ (Materials Image Processing and Automated Reconstruction) [6] was utilized for the data segmentation. 'Recipes' were created within the image processor of MIPAR™ to create a series of steps that segment the grayscale image into a binary image [6]. These recipes were then applied to 600 of the TIF images through use of the batch processor in MIPAR™, and later manually edited individually in the processed image editor of MIPAR™ to maximize accuracy.

In total, the dentin microtubules, nanotubules, and peritubular dentin were all independently segmented. Then each of these features were reconstructed into individual 3D models as well as a single model including all the features.

Measurements were taken from the data in two ways. The first method involved taking measurements of every slice using MIPAR™. The areas of the intertubular dentin, microtubules, nanotubules, and peritubular dentin were all recorded along with the number of microtubules per slice. The microtubules' diameters were measured by morphing every microtubule into an ellipse and recording the major axis length (Table 1). The nanotubules' lengths were measured by use of Feret's diameter (Table 1) which tries to make the largest line possible within each nanotubular feature, much like a dial caliper.

The second group of measurements were taken using the 3D reconstruction in Avizo. Individual microtubules and the nanotubules branching from them were segmented from the rest of the model. The nanotubules were then measured in quantity as well as length and diameter using the 'Label Analysis' feature (Table 2). This was done for 10 different microtubules at various locations throughout the model, but all spanned the entire length of the sample, from slide 1 to 601.

Results & Discussion

The 3D reconstruction clearly showed that there is a network of nanotubules that connect the microtubules together with an average of about 17 nanotubules branching off each microtubule. The nanotubules connect both microtubules in close proximity and otherwise. The nanotubules do not always span to another microtubule but sometimes terminate within the intertubular dentin or peritubular dentin. The nanotubules seem to curve away from microtubules that it does not make contact with, as seen below in Figure 1. Some nanotubules are also connected to one another and are observed to branch in 'Y' shapes.

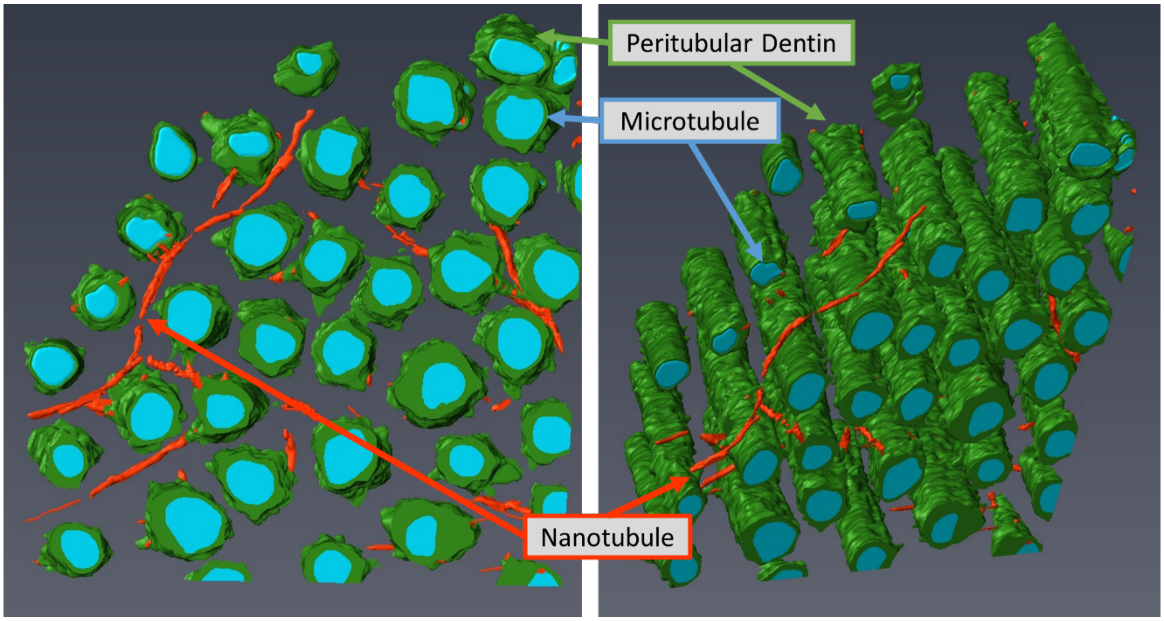

Figure 1: Portion of the 3D reconstruction, which includes the microtubules, nanotubules, and peritubular dentin.

The size of the microtubules and nanotubules seem to correlate (Figure 2) with the depth of the dentin as well as the percent composition. There appears to be a negative correlation between the area of the peritubular dentin and microtubules as one approaches the dentin enamel junction (Figure 2). More samples need to be analyzed to confirm whether this is a universal trend. This trend is likely due to the chemical etching that was performed on the sample.

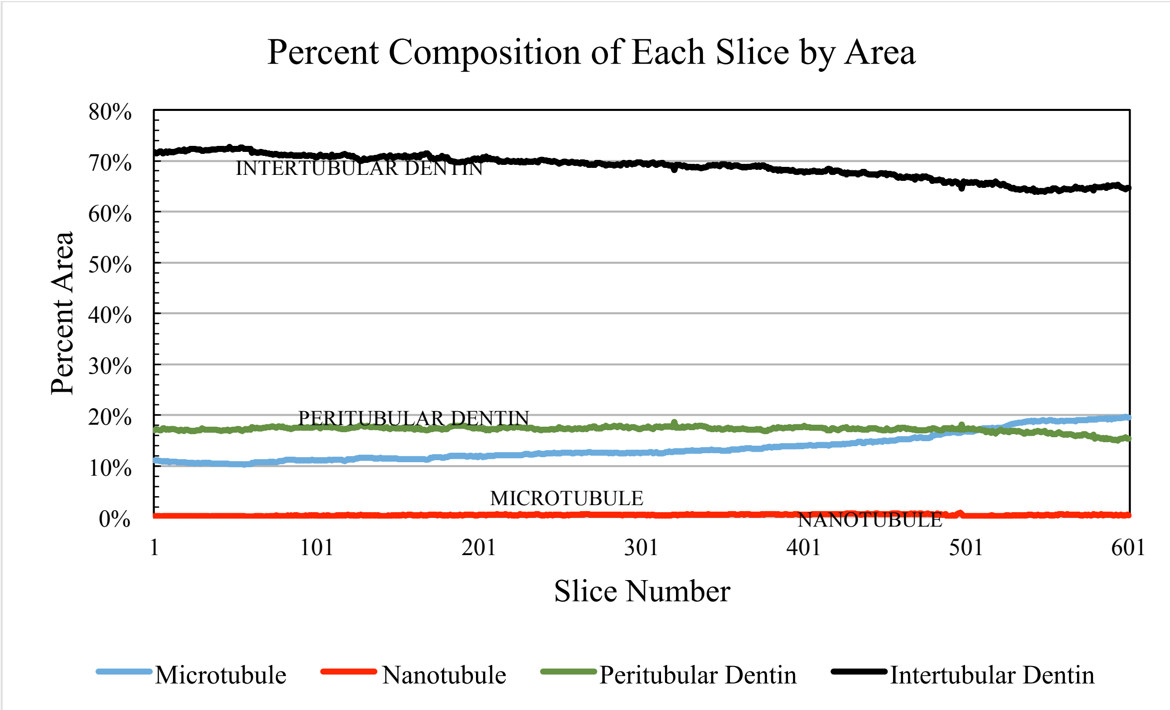

Figure 2: Plot of percent composition of features within each slice in terms of area. Slice 1 being closer to the pulp, and slice 601 being closer to the enamel. About 38.24 microns in total depth.

The 2D analysis, below, shows an increase in the average microtubule diameter and average nanotubule length as one approaches the enamel. The microtubules had an average diameter of 2.75 μm (Table 1). There is great confidence in the microtubule diameter since each slice is perpendicular to the microtubule, however, the measured nanotubule length is not as accurate because the slices are more or less parallel to them. This causes only small portions of each nanotubule to be measured in each slice. The nanotubules are much more accurately measured in the 3D analysis (see Table 2). There is a lower risk of only partially measuring each nanotubule many times in the 3D analysis because the entire length and width of the 3D model of the nanotubule was measured leading to a more accurate measurement. The 2D analysis showed the average length of the nanotubules 582 nm whereas the 3D analysis shows an average length of 696 nm.

Table 1: 2D analysis of all slices. Microtubule diameter was measured by morphing each microtubule into an ellipse and recording the major axis length. Nanotubule length was measure by use of Feret's diameter.

Slides	Approx. Depth in	Microtubule Average Major Axis Length (μm)	Nanotubule Average Feret's Diameter (nm)

	Dentin (µm)		
1-50	36.8	2.484	541
51-100	33.6	2.501	514
101-150	30.4	2.546	508
151-200	27.2	2.563	552
201-250	24	2.581	554
251-300	20.8	2.634	570
301-350	17.6	2.666	519
351-400	14.4	2.781	533
401-450	11.2	2.834	531
451-500	8	2.941	612
501-550	4.8	3.140	767
551-601	1.6	3.325	786
Average		**2.750**	**582**

Table 2: 3D Analysis of Nanotubules. Average of the nanotubules coming off of 10 microtubules.

Nanotubule Size		
	Length (nm)	Diameter (nm)
Average Minimum	135	70
Average Maximum	3270	922
Average of All 10	**695**	**208**

Conclusion

The microtubules had an average diameter of 2.75 µm (Table 1). Every observed microtubule did have multiple nanotubules (avg. of 17) branching off of it. The length the nanotubules span is significantly different, from 135 nm to 3270 nm on average (Table 2). Some nanotubules interconnected with one another creating a network between microtubules and others did not. The trends observed in percent area composition (Figure 2) are not convincing in and of themselves, but could lead to interesting insight upon repeating the procedure on more samples.

However, the segmentation of the features, especially the nanotubules, proved to be difficult and time intensive. This is due to their small size and the fact that they are an area of negative space just like the microtubules. Better imaging techniques and sample preparation could aid in this process. For example, pouring a resin into the sample to fill the micro/nanotubules could help during segmentation.

Future research will involve analyzing more samples at an increased depth range to confirm or refute the trends seen in Figure 1 and Chart 1, and possibly conducting a flow simulation of the 3D rendered model to assess the validity of the hydrodynamic theory.

References

1. Arnold, W.H., and P. Gaengler. "Quantitative analysis of the calcium and phosphorus content of developing and permanent human teeth." Annals of Anatomy, vol. 189, no. 2, 2007, pp. 183-190. OhioLINK Electronic Journal Center, doi:10.1016/J.AANAT.2006.09.008
2. Coutinho, Eduardo Tavares, d'Almeida, José Roberto Moraes, & Paciornik, Sidnei. (2007). "Evaluation of microstructural parameters of human dentin by digital image analysis." *Materials Research*, *10*(2), 153-159
3. Dominic Barron, (iii) Basic science: computed tomography, Current Orthopaedics, Volume 19, Issue 1, 2005, Pages 20-26, ISSN 0268-0890.
4. Parkinson, Charles R, and Alexander Sasov. "High-resolution Non-Destructive 3d Interrogation of Dentin Using X-Ray Nanotomography." *Dental Materials*. 24.6 (2008): 773-777. Print.
5. Shiau, Harlan J., DDS, DMSc. "Dentin Hypersensitivity." The Journal of Evidence-Based Dental Practice, vol. 12, no. 3, 2012, pp. 220-228. OhioLINK Electronic Journal Center, doi:10.1016/S1532-3382(12)70043-X
6. Sosa, John M, Daniel E. Huber, Brian Welk, and Hamish L. Fraser. "Development and Application of MIPAR™: a Novel Software Package for Two and Three-Dimensional Microstructural Characterization." *Integrating Materials and Manufacturing Innovation*. 3.1 (2014). Print.
7. Zaslansky, Paul, Simon Zabler, and Peter Fratzl. "3d Variations in Human Crown Dentin Tubule Orientation: a Phase-Contrast Microtomography Study." *Dental Materials*. 26.1 (2010). Print.